Numerical power balance and free energy loss analysis for solar cells including optical, thermodynamic, and electrical aspects

Johannes Greulich,[a] Hannes Höffler, Uli Würfel, and Stefan Rein
Fraunhofer Institute for Solar Energy Systems, Heidenhofstr. 2, D-79110 Freiburg, Germany

(Received 19 September 2013; accepted 6 November 2013; published online 26 November 2013)

A method for analyzing the power losses of solar cells is presented, supplying a complete balance of the incident power, the optical, thermodynamic, and electrical power losses and the electrical output power. The involved quantities have the dimension of a power density (units: W/m^2), which permits their direct comparison. In order to avoid the over-representation of losses arising from the ultraviolet part of the solar spectrum, a method for the analysis of the electrical free energy losses is extended to include optical losses. This extended analysis does not focus on the incident solar power of, e.g., 1000 W/m^2 and does not explicitly include the thermalization losses and losses due to the generation of entropy. Instead, the usable power, i.e., the free energy or electro-chemical potential of the electron-hole pairs is set as reference value, thereby, overcoming the ambiguities of the power balance. Both methods, the power balance and the free energy loss analysis, are carried out exemplarily for a monocrystalline *p*-type silicon metal wrap through solar cell with passivated emitter and rear (MWT-PERC) based on optical and electrical measurements and numerical modeling. The methods give interesting insights in photovoltaic (PV) energy conversion, provide quantitative analyses of all loss mechanisms, and supply the basis for the systematic technological improvement of the device. © *2013 AIP Publishing LLC*. [http://dx.doi.org/10.1063/1.4832777]

I. INTRODUCTION

The maximum efficiency of solar cells and the analysis of its limiting factors have been the topic of research for many years.[1–7] These publications focus on idealized solar cells, i.e., devices, which feature only intrinsic, unavoidable loss mechanisms, such as free-carrier absorption, radiative and Auger recombination, and thermodynamic aspects, such as the generation of entropy. In real solar cells, additional losses occur, which are caused by extrinsic mechanisms, e.g., the reflection of incident photons, non-radiative, non-Auger recombination as Shockley-Read-Hall recombination, and series resistance. Recently, Brendel *et al.*[8] presented a method for analyzing the free energy losses caused by electrical effects (recombination and transport of electrons and holes), which allows to compare the losses directly, since they are quantified in the same units. This method is based on numerical device simulations. It has been applied to real, i.e., non-idealized solar cells.[9–13] However, this method covers only the electrical losses.

In this manuscript, we consider two methods for analyzing the losses of real, i.e., non-idealized photovoltaic devices. Both methods are exemplarily applied to a solar cell based on monocrystalline *p*-type silicon. Section II focusses on a power loss analysis, henceforth called power balance, including optical, thermodynamic, and electrical aspects. A general method is presented, which balances the incident power of the solar radiation, the various kinds of power losses, and the electrical output power. In Sec. III, Brendel's electrical free energy loss analysis[8] is extended to include also optical effects. In contrast to the power balance presented in Sec. II, this method does not relate the losses to the incident power of the solar radiation. Instead, the usable power, i.e., the free energy or electro-chemical potential of the electron-hole pairs is set as reference value. Thereby, the over-representation of the ultra-violet part of the solar spectrum caused by weighting each reflected photon with its energy and the resulting ambiguities of the power balance discussed in Sec. II A are overcome. All optical and electrical loss channels are quantified in units of W/m^2, which makes them directly comparable.

Both methods, the power balance and the extended free energy loss analysis, are carried out exemplarily for a monocrystalline large-area *p*-type silicon metal wrap through passivated emitter and rear cell (MWT-PERC) described in Refs. 14 and 15. The analysis permits to identify promising approaches for future improvements of the MWT-PERC structure.

II. POWER BALANCE

The power balance follows the temporal sequence of photovoltaic energy conversion, which begins with the optical part, i.e., the reflection and the absorption of photons, and the generation of hot charge carriers, which have a rather high mean kinetic energy representing the energy distribution of the absorbed photons, i.e., the temperature of the sun. This is followed by the thermodynamic part, which comprises losses due to the thermalization or "cooling" of the generated hot charge carriers until their energies approach the band edges, and the entropy of the ensembles of thermalized electrons and holes. Finally, the recombination inside the device and the transport of thermalized charge carriers to the device terminals, where the electrical power is delivered,

[a]Author to whom correspondence should be addressed. Electronic mail: johannes.greulich@ise.fraunhofer.de. Tel.: +49-761-4588-5488. Fax: +49-761-4588-7812.

constitute the electrical part. This temporal sequence is represented in Secs. II A–II C covering the optical, thermodynamic, and electrical losses. The method is then applied to a MWT-PERC.

A. Optics

Following the temporal sequence, this first section deals with the question how efficiently the solar spectrum is exploited by the optical properties of the device. The amount of usable energy is reduced due to reflection of photons at the front side and parasitic absorption of photons, e.g., within dielectric passivation layers.

The spectrum of the incident illumination, which may be, e.g., the AM1.5g solar spectrum,[16] is denoted in the following with $\phi(\lambda)$ and is given in units of W/m^2/nm. The reflectance $R(\lambda)$ of the device is a measurable quantity, which causes a power loss of

$$P_{\mathrm{refl}} = \int_0^\infty \phi(\lambda) \cdot R(\lambda) \cdot d\lambda. \tag{1}$$

The power that is absorbed in the anti-reflection coating ($y = \mathrm{ARC}$), in the front metallization ($y = \mathrm{FM}$), in the rear metallization ($y = \mathrm{RM}$), and in the silicon due to band-band absorption ($y = \mathrm{BB}$), or due to free carriers ($y = \mathrm{FCA}$) has to be considered, which requires optical simulation. The power losses for the above loss channels are given by

$$P_{\mathrm{abs},y} = \int_0^\infty \phi(\lambda) \cdot A_y(\lambda) \cdot d\lambda. \tag{2}$$

The power conversion due to band-band absorption $P_{\mathrm{abs,\,BB}}$ is the power of the generated electron-hole pairs, which is finally partly converted into electrical output power and should not be understood as a loss. The absorptance $A_y(\lambda)$ is defined as the ratio of the number of photons that are absorbed, e.g., in the anti-reflection coating ($y = \mathrm{ARC}$), and the number of photons incident onto the solar cell. A_{ARC}, A_{BB}, A_{FM}, A_{RM}, and A_{FCA} are quantities that are accessible by optical simulations and may each depend on other properties of the solar cell. For example, the absorptance of the rear metallization depends on the number of photons that reach the rear surface, i.e., A_{RM} depends on, e.g., the wafer thickness and the design of the anti-reflection coating.

Inserting the incident power spectrum $\phi(\lambda)$ (given in W/m^2/nm or eV/s/m^2/nm) instead of, e.g., the photon flux $\phi(\lambda)/E_\gamma$ (given in photons/s/m^2) implies that integrating the input spectrum with respect to the wavelength gives under standard testing conditions the input power of 1000 W/m^2 and that, e.g., each reflected photon induces an energy loss of $E_\gamma = h \cdot c/\lambda$. This agrees with the temporal sequence of PV energy conversion, since the power of 1000 W/m^2 is incident onto the device under standard testing conditions and, e.g., each reflected photon carries the energy E_γ. However, inserting the power instead of, e.g., the photon flux may result in misleading interpretations of the power balance for the following reason. According to the presented formulas (1) and (2), a reflected or parasitically absorbed high-energy photon with an energy of, e.g., 4 eV ($\lambda = 310$ nm) appears as a twice as large power loss as a low-energy photon with an energy of, e.g., 2 eV ($\lambda = 620$ nm), although each photon could generate only a single electron-hole pair if it was absorbed within the silicon. This has to be kept in mind, since otherwise the method may give misleading hints for the device optimization. This point is addressed also in Sec. III, where a method is proposed that weighs each photon with the free energy it would create if it was absorbed within the silicon.

B. Thermodynamics

Once the photons are absorbed within the silicon by generating electron-hole pairs, the temporal sequence of photovoltaic energy conversion continues with the thermodynamic losses. These comprise the thermalization of charge carriers towards the band edges and the generation of entropy (see Figure 1).

The generated free charge carriers have a large kinetic energy if the photon's energy is larger than the band gap. In today's industrially produced solar cells, a large fraction of the kinetic energy is lost due to scattering at the lattice of the crystal until the electron gas temperature reaches the lattice temperature, e.g., 300 K. This happens after few picoseconds (Ref. 17, p. 309) and is known as thermalization or "cooling" of hot charge carriers (see Figure 1). In principle, this loss could be reduced, e.g., by using absorbers with multiple band gaps or multi-junction solar cells (Ref. 17, p. 297ff). In this case, the presented thermodynamic part of the power balance has to be applied to each individual sub-cell. Also, the thermalization loss can be reduced with a hot carrier device (Ref. 17, p. 309ff), where the thermalization of the

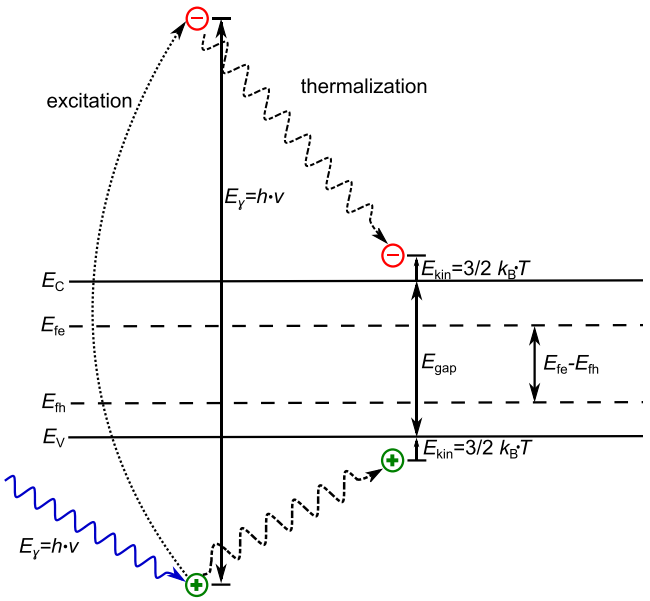

FIG. 1. The band diagram in the energy-position space shows (from left to right) the following steps: A high-energy photon excites an electron from the valence band to the conduction band leaving a hole in the valence band. A part of the photon's energy $h \cdot \nu$ is lost due to thermalization of the charge carriers close to the band edges. The usable free energy per electron-hole pair does not correspond to the energy difference of the states occupied by the electron and hole after thermalization, but is given by the splitting of the quasi-Fermi energies E_{fe}–E_{fh}.

charge carriers must not be complete before their extraction. Since these devices are still far from industrial production, they are not treated in the present analysis. However, the methodology presented here can be adapted to the needs of hot carrier devices.

After the thermalization, the excited electrons and holes remain in the conduction and valence band, respectively, for typically some micro- to milli-seconds before they recombine or are extracted. These excited electrons (holes) in the conduction (valence) band are usually described as being in quasi-thermal equilibrium with each other and with the lattice. For the general case of Fermi-Dirac statistics, the mean energy of such a charge carrier is given by (Ref. 18, p. 44 and Ref. 19, p. 232)

$$\begin{aligned}\langle E_e\rangle &= \frac{1}{n_e}\int_{E_c}^{\infty} E_e \cdot D_e(E_e)\cdot f_e \cdot dE_e \\ &= E_c + \frac{3}{2}\cdot k_B \cdot T \cdot \frac{f_{3/2}[(E_{fe}-E_c)/(k_B T)]}{f_{1/2}[(E_{fe}-E_c)/(k_B T)]}, \end{aligned} \quad (3)$$

for electrons and

$$\begin{aligned}\langle E_h\rangle &= \frac{1}{n_h}\int_{-\infty}^{E_v} E_h \cdot D_h(E_h)\cdot f_h \cdot dE_h \\ &= -E_v + \frac{3}{2}\cdot k_B \cdot T \cdot \frac{f_{3/2}[(E_v-E_{fh})/(k_B T)]}{f_{1/2}[(E_v-E_{fh})/(k_B T)]}, \end{aligned} \quad (4)$$

for holes, with $n_{e/h}$ being the density of electrons/holes, $E_{e/h}$ the energy of electrons/holes, $D_{e/h}$ their density of states, $f_{e/h}$ their occupation probability in the conduction/valence band, respectively, $E_{f\,e/h}$ their quasi-Fermi energies, $E_{c/v}$ the energy of the conduction/valence band edge, and k_B Boltzmann's constant. The Fermi-Dirac integral is defined as

$$f_\nu(x) = \frac{1}{\Gamma(\nu+1)}\int_0^\infty \frac{t^\nu}{\exp(t-x)+1}dt, \quad (5)$$

with $t = (E-E_c)/(k_B\cdot T)$ for electrons and $t = (E_v - E)/(k_B\cdot T)$ for holes (Ref. 19, p. 231). In the case of $E_c - E_{fe} \gg k_B\cdot T$ and $E_{fh} - E_v \gg k_B\cdot T$, i.e., for carrier densities much smaller than the effective densities of states N_c and N_v (approx. $3\times 10^{19}\,\mathrm{cm}^{-3}$ for silicon at $T = 300\,\mathrm{K}$ (Ref. 20)), Boltzmann statistics can be applied. Then, the quotient of the Fermi-Dirac integrals in Eqs. (3) and (4) cancels (Ref. 18, pp. 44, 46, and 56), which simplifies the practical computation. Accordingly, each electron-hole pair carries after the thermalization only the mean energy (assuming Boltzmann statistics)

$$\langle E\rangle = \langle E_e\rangle + \langle E_h\rangle = E_{gap} + 3\cdot k_B\cdot T, \quad (6)$$

which is slightly larger than the band gap due to the kinetic energy of electrons and holes. This mean energy $\langle E\rangle$ after thermalization is only a fraction of the photon's energy $E_\gamma(\lambda)$, which equals the energy of the electron-hole pair before thermalization. Based on Eqs. (2) and (6), the power loss due to thermalization can be written as

$$\begin{aligned}P_{therm} &= \int_0^\infty \phi(\lambda)\cdot A_{BB}(\lambda)\cdot\left\{1-\frac{\langle E\rangle}{E_\gamma(\lambda)}\right\}\cdot d\lambda \\ &= \int_0^\infty \phi(\lambda)\cdot A_{BB}(\lambda)\cdot\left\{1-\frac{E_{gap}+3k_B T}{\frac{h\cdot c}{\lambda}}\right\}\cdot d\lambda. \end{aligned} \quad (7)$$

The solar cell can deliver only a fraction of this energy as work to an external load. Since the temperature and the volume of the thermalized electron and hole gases are assumed constant, the Helmholtz free energy $F(T,V,N) = E(S,V,N) - T\cdot S$ of electrons and holes is the relevant thermodynamic potential. When generating dN electron-hole pairs within the device, the free energies of the electron and of the hole gases change by

$$\begin{aligned}dF_e &= E_{fe}\cdot dN \\ dF_h &= -E_{fh}\cdot dN, \end{aligned} \quad (8)$$

since the temperature and the volume are constant during cell operation ($dT = dV = 0$) (see Figure 1 and Ref. 18, p. 57). Adding electrons and holes gives the amount of free energy carried by dN generated electron-hole pairs, which is given by the difference of the quasi-Fermi energies

$$dF = dF_e + dF_h = (E_{fe} - E_{fh})dN = \Delta\eta\cdot dN, \quad (9)$$

where the difference of the quasi-Fermi energies is abbreviated with $\Delta\eta = E_{fe} - E_{fh}$. This quantity depends on the generation, recombination and extraction of charge carriers and therefore on the operating voltage of the device, which may be chosen to match the voltage of maximum power. The thermodynamic power loss per generated electron-hole pair associated with the generation of entropy of the electron and hole gases thus corresponds to the difference of the mean internal energy $\langle E\rangle$ and $\Delta\eta$. The power loss associated with the entropy can be expressed as

$$P_{entropy} = \frac{1}{A}\cdot\int_V \{E_{gap} + 3\cdot k_B\cdot T - \Delta\eta(x,y,z)\}\cdot G(x,y,z)\cdot dV, \quad (10)$$

where the integration is performed over the volume V of the solar cell, which has a surface area A. The spatial generation rate of electron-hole pairs is denoted with $G(x,y,z)$ and may include spatial inhomogeneities, e.g., caused by the device geometry and by shading due to the front side metallization. This power loss corresponds to the heat of the electron and hole gases, which is unusable in terms of the electrical energy delivered by the photovoltaic device. It is partially caused by recombination, but is not identical to it, since $\Delta\eta$ depends also on the charge carrier extraction and the operating voltage of the device.

The rate at which free energy density is generated within the solar cell has the dimension power/area and is given by

$$P_g = \frac{1}{A}\cdot\int_V \Delta\eta(x,y,z)\cdot G(x,y,z)\cdot dV. \quad (11)$$

Since the splitting of the quasi-Fermi energies $\Delta\eta = E_{fe} - E_{fh}$ and the band-band absorptance A_{BB} are included in these calculations, the thermalization loss, the free energy generation rate and the entropy generation rate can be calculated only based on optical and electrical simulations.

C. Electrics

The third and last part of the temporal sequence of photovoltaic energy conversion concerns the electrics, i.e., the recombination and transport of electrons and holes within the semiconductor. The losses and the respective quantities (recombination rate, current densities,…) can be evaluated in principle at each point of the cell's current-voltage characteristic. The most important is certainly the maximum power point (mpp). The subsequent electrical part of the power loss analysis is based on the work of Brendel *et al.*[8]

The power extracted from the solar cell

$$P_{ex} = j \cdot V = P_g - P_r - P_{t,e} - P_{t,h} - P_s, \tag{12}$$

is given by the product of the electrical current density j and the voltage V at the device's terminals, which in turn is given by balancing the following free energy generation/dissipation rates.

The free energy generation rate P_g is given by Eq. (11).

The power loss or free energy density dissipation rate due to recombination in the semiconductor

$$P_r = \frac{1}{A} \cdot \int_V \Delta\eta(x,y,z) \cdot r(x,y,z) \cdot dV, \tag{13}$$

depends directly on the total recombination rate r, to which all recombination channels (Shockley-Read-Hall, Auger, radiative,…) contribute. Furthermore, recombination reduces the splitting of the quasi-Fermi energies $\Delta\eta(x,y,z)$ and thus contributes also indirectly to the power loss due to recombination and to the power loss associated with entropy (see Sec. II B). Remember that $\Delta\eta(x,y,z) = E_{fe}(x,y,z) - E_{fh}(x,y,z)$ depends also on the charge carrier extraction/operating voltage of the device. The integration is performed on all cell regions (e.g., emitter, base, back surface field).

The power loss or free energy density dissipation rate due to recombination at the non-contacted surfaces (∂V_{nc}), at the surfaces of the n-type contact where electrons are extracted (∂V_e) and at the p-type contact where holes are extracted (∂V_h) is given by

$$\begin{aligned} P_s = &\frac{1}{A} \cdot \int_{\partial V_{nc}} \Delta\eta(x,y,z) \cdot \frac{\vec{j}_h(x,y,z)}{(+q)} \cdot d\vec{A} \\ &+ \frac{1}{A} \cdot \int_{\partial V_e} \Delta\eta(x,y,z) \cdot \frac{\vec{j}_h(x,y,z)}{(+q)} \cdot d\vec{A} \\ &+ \frac{1}{A} \cdot \int_{\partial V_h} \Delta\eta(x,y,z) \cdot \frac{\vec{j}_e(x,y,z)}{(-q)} \cdot d\vec{A}. \end{aligned} \tag{14}$$

Here, the components of the electron and hole current densities within the simulation domain normal to its surfaces $\vec{j}_{e/h} \cdot d\vec{A}$ correspond to the surface recombination rates of minority charge carriers at the respective surfaces and do not represent the extracted current densities. The local quasi-Fermi level splitting $\Delta\eta(x,y,z) = E_{fe}(x,y,z) - E_{fh}(x,y,z)$ corresponds to the lost free energy per charge carrier pair.

Finally, the transport of electrons and holes within the semiconductor via drift and diffusion induces additional free energy density dissipation rates

$$P_{t,e} = \frac{1}{A} \cdot \int_V \frac{\left|\vec{j}_e(x,y,z)\right|^2}{\sigma_e} \cdot dV + R_{s,e} \cdot j^2 \tag{15}$$

and

$$P_{t,h} = \frac{1}{A} \cdot \int_V \frac{\left|\vec{j}_h(x,y,z)\right|^2}{\sigma_h} \cdot dV + R_{s,h} \cdot j^2, \tag{16}$$

respectively. The local electron and hole current densities within the simulation domain at the positions with the coordinates (x, y, z) are denoted with $\vec{j}_{e/h}$ and the respective electrical conductivities of the semiconductor with $\sigma_{e/h}$. Again, the volume V contains all cell regions (e.g., emitter, base,…). The integrals in Eqs. (15) and (16) are derived in Ref. 8. They correspond to the Ohmic power losses $P = U \cdot I = (R \cdot I) \cdot I = R \cdot I^2$ due to heating caused by an electrical current I passing through a resistor R at a voltage U. Equations (15) and (16) are altered compared to those given by Brendel *et al.*[8] by the second summand in each equation. This term is composed by the current density j extracted from the solar cell at the given bias, e.g., at the maximum power point of the current-voltage curve ($j = j_{mpp}$) and several contributions to the effective series resistance for electrons ($R_{s,e}$) and holes ($R_{s,h}$), which may not directly be included in the numerical simulation domain. This allows these power losses at the lumped series resistance to be taken into account as lumped parameter. Please note that the current density j is the current extracted from the simulation domain divided by its surface area, and must not be confused with the local electron and hole current densities $\vec{j}_{e/h}(x,y,z)$ at the position (x, y, z) within the simulation domain.

D. Application of the power balance to a MWT-PERC

The method is exemplarily applied to a metal wrap through solar cell with passivated emitter and rear (MWT-PERC). Since the calculations involve in large part quantities that are not accessible by measurements, they are based on numerical, optical, and electrical modeling of the device using Sentaurus TCAD.[22] Since the cell features three rows of vias, only a third of the device's cross section is sketched in Figure 2. The cell thickness is 160 μm, and its top surface area is 149 cm^2. The optical simulations involve a ray-tracing approach, including the geometry of the front surface texture and the rear surface roughness, and interference at the thin dielectric layers at the front and rear surface.[23,24] Band-to-band absorption in silicon with absorption coefficient α_{BB} is modeled based on the refractive indices given by Green.[25] Free-carrier absorption is taken into account using the empirical parameterization by Rüdiger *et al.*[26] for the absorption coefficient α_{FCA}. The spectral

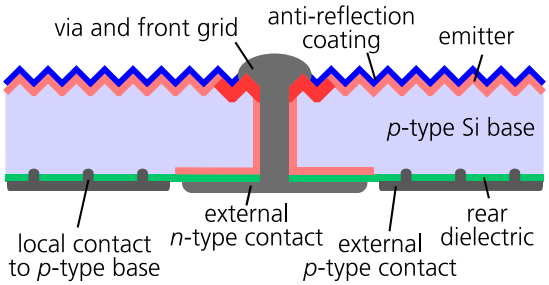

FIG. 2. The sketch of the cross-section of a third of the monocrystalline *p*-type MWT-PERC analyzed in this paper (not to scale). The front side features an *n*-type selective emitter structure. The front metallization is wrapped through the wafer at the vias. The screen printed *p*-type contact is locally connected to the rear of the base via laser-fired-contacts.[21] The front and rear surfaces are passivated by a thermally grown silicon oxide.

charge carrier generation rate $G(x, y, z, \lambda)$ due to band-to-band absorption and the spectral rate of free-carrier absorption $A_{\mathrm{FCA}}(x, y, z, \lambda)$ are calculated from the total spectral absorption rate $A_{\mathrm{tot}}(x, y, z, \lambda)$ at the position (x, y, z) within the silicon for the wavelength λ as

$$G(x,y,z,\lambda) = \frac{\alpha_{\mathrm{BB}}(\lambda)}{\alpha_{\mathrm{BB}}(\lambda)+\alpha_{\mathrm{FCA}}(\lambda)} \cdot A_{\mathrm{tot}}(x,y,z,\lambda)$$
$$A_{\mathrm{FCA}}(x,y,z,\lambda) = \frac{\alpha_{\mathrm{FCA}}(\lambda)}{\alpha_{\mathrm{BB}}(\lambda)+\alpha_{\mathrm{FCA}}(\lambda)} \cdot A_{\mathrm{tot}}(x,y,z,\lambda). \quad (17)$$

The optics are calibrated by comparing the simulated to the measured spectral hemispherical reflectance. Therefore, the simulated and measured reflectance data can be used interchangeable. However, the optical simulation is needed to calculate all other optical losses and the charge carrier generation rate. For the electrical simulations, the Poisson equation and the continuity equations for electrons and holes are solved numerically. Lifetime samples are prepared parallel to the cell batch in order to determine the saturation current density of the *n*-type emitter, the bulk lifetime and the recombination velocity of the passivated rear surface. An effective emitter with a saturation current density $j_{0e} = 150$ fA/cm^2 is applied according to the measurement on lifetime samples processed parallel to the device. The bulk recombination in the Czochralski-grown, *p*-type silicon wafer with a resistivity of 1.8 Ω cm is dominated by Auger recombination, since the boron-oxygen defect has been deactivated. Based on measurements[15] and analytical modeling,[27] an effective rear surface recombination velocity of 160 cm/s has been estimated.[14] With these inputs, the measured energy conversion efficiency of more than 20% is reproduced by the simulations. Further details can be found in Ref. 14.

The analysis is carried out for the maximum power point of the current-voltage characteristics under 1 sun illumination (1000 W/m^2) with the AM1.5g spectrum[16] for a solar cell temperature of 300 K. The spectral reflectance and the output power of the device are directly measured, whereas other input data are simulated based on other measurements, as explained above. The direct comparison of all power losses shown in Figure 3 summarizes the findings of the power balance evaluation. 202 W/m^2 of the incident 1000 W/m^2 are converted into electrical output power,

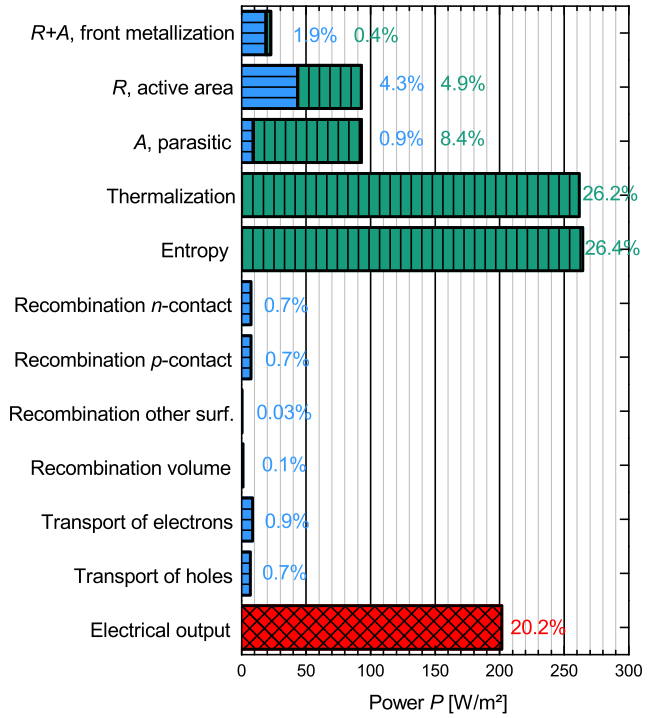

FIG. 3. The complete power balance of the incident 1000 W/m^2 is applied to a MWT-PERC at the maximum power point of the current-voltage characteristics. It includes different loss channels. 202 W/m^2 of the incident power are converted into electrical output power (red bar) corresponding to the energy conversion efficiency of 20.2%. The losses caused by inherent material properties of silicon and the losses arising from those parts of the solar spectrum, which are outside the sensitive spectral range of silicon (green bars, vertically hatched) are by far larger than the losses that can be modified technologically (blue bars, horizontally hatched).

corresponding to a conversion efficiency of 20.2%. The largest losses arise from thermalization of generated charge carriers to the band edges (262 W/m^2) and from the creation of entropy (264 W/m^2), which is directly reflected in the difference between the band gap energy and the splitting of the quasi-Fermi energies. The thermalization loss is unavoidable and cannot be reduced to zero if we restrict ourselves to single-junction, wafer-based solar cells and the solar illumination spectrum. The creation of entropy cannot be avoided completely but partly by increasing the splitting of the quasi-Fermi levels. This in turn cannot be done directly, but indirectly by reducing the charge carrier recombination. However, a certain amount of entropy at the maximum power point is mandatory because the transport of the charge carriers to the external contacts of the solar cell requires a gradient of the quasi-Fermi levels.

A large optical loss is parasitic absorption (93 W/m^2), which occurs mainly above 1.2 μm, i.e., outside the spectral range that can be absorbed by the semiconductor silicon. The reflectance of the active cell area below 1.2 μm (blue bars, horizontally hatched in Figure 3) constitutes the largest relevant and technologically accessible loss. This loss has to be optimized conjointly with the thermalization loss for the following reason. With the presented power balance, more weight is given to high-energy photons than to low-energy photons. Therefore, the optical loss due to the reflection of the active cell area can, in principle, be reduced by

optimizing the anti-reflection coating for the ultraviolet part of the solar spectrum. This, in turn, will increase the thermalization loss of the electron-hole pairs excited by high-energy photons. This interdependence is clearly a drawback of the presented method.

A second drawback concerns the sequence of applying the loss mechanisms. The sequence chosen here is justified by following the sequence of photovoltaic energy conversion. If the sequence of applying the different loss mechanisms (e.g., due to thermalization and reflection) was changed, the apportionment of the losses would have changed (e.g., if thermalization losses were applied to all incident photons, not only to the photons generating electron-hole pairs).

These drawbacks of the presented power balance are overcome in Sec. III by the free energy analysis. Nevertheless, this power balance, besides motivating the free energy analysis, can be used to relate the electrical output power, the fundamental losses, and the technologically accessible losses to one another, giving interesting insights in the process of photovoltaic energy conversion.

III. OPTICAL AND ELECTRICAL FREE ENERGY LOSS ANALYSIS

In the power balance presented in Sec. II, the power losses have been related to the incident power of $1000\,\mathrm{W/m^2}$. However, the presented approach leads to results, which may be misleading for two reasons. First, although each photon typically can generate only one electron-hole pair, the lost photons are weighted depending on the wavelength by the respective photon energy $E_\gamma = h{\cdot}c/\lambda$, since the intensity, not the photon flux, e.g., is used. Second, optical and thermodynamic losses (e.g., reflection and thermalization) are strongly correlated with each other within the presented formalism. In the present section, a different approach is developed. The center of the present analysis is the free energy or the electro-chemical potential of electrons and holes. The analyzed losses are related to this quantity. As argued in Sec. II B, the free energy is the usable amount of energy. Losses due to thermalization or generation of entropy are not relevant for this kind of analysis, since the free energy is free of entropy.

A. Optical part

As already given above by Eq. (11), the rate at which free energy density is generated within the solar cell is given in $\mathrm{W/m^2}$ by

$$P_\mathrm{g} = \frac{1}{A} \cdot \int_V \Delta\eta(x,y,z) \cdot G(x,y,z) \cdot dV, \tag{18}$$

where the splitting of the quasi-Fermi energies $\Delta\eta$ corresponds to the splitting of the electro-chemical potentials of electrons and holes. The rate at which electron-hole pairs are generated upon illumination with the spectrum $\phi(\lambda)$ is given by the charge carrier generation rate

$$G(x,y,z) = \int_0^\infty \phi(\lambda) \cdot g(x,y,z,\lambda) \cdot d\lambda, \tag{19}$$

where $g(x, y, z, \lambda)$ denotes the spectral generation normalized to the incident intensity $\phi(\lambda)$. Thus, the rate of free energy generation in the solar cell's volume V can be written by inserting Eq. (19) into Eq. (18) as

$$P_\mathrm{g} = \frac{1}{A} \cdot \int_V \Delta\eta(x,y,z) \cdot \int_0^\infty \phi(\lambda) \cdot g(x,y,z,\lambda) \cdot d\lambda \cdot dV. \tag{20}$$

The free energy of every photon that is lost due to reflection or parasitical absorption is given by the free energy of the electron-hole pair that the photon would generate if it was absorbed within the silicon. Therefore, the rate at which free energy is lost due to reflection of light by the device is written analogously to Eq. (20) as

$$\dot{f}_\mathrm{refl} = \frac{1}{A} \cdot \int_V \Delta\eta(x,y,z) \cdot \int_0^\infty \phi(\lambda) \cdot g(x,y,z,\lambda) \cdot R(\lambda) \cdot d\lambda \cdot dV, \tag{21}$$

where again the reflectance is denoted with $R(\lambda)$.

The rate at which free energy is absorbed in the anti-reflection coating ($y = \mathrm{ARC}$), in the front metallization ($y = \mathrm{FM}$), in the rear metallization ($y = \mathrm{RM}$), and in the silicon due to band-band absorption ($y = \mathrm{BB}$), or due to free carriers ($y = \mathrm{FCA}$) is given by

$$\dot{f}_{\mathrm{abs},y} = \frac{1}{A} \cdot \int_V \Delta\eta(x,y,z) \cdot \int_0^\infty \phi(\lambda) \cdot g(x,y,z,\lambda) \cdot A_y(\lambda) \cdot d\lambda \cdot dV. \tag{22}$$

B. Electrical part

The electrical part of the free energy analysis is the same as described in Sec. II C, which is based on the work of Brendel *et al.*,[8] and is given by Eqs. (12)–(16).

As argued above, the loss channels, e.g., the optical and thermodynamic losses in the case of the energy balance are strongly correlated with each other. In contrast, the recombination channels in the free energy loss analysis are not as strongly correlated with each other. However, they are still slightly correlated, as is illustrated in the following. Reducing one kind of loss by a certain amount of power does not increase the electrical output power by the same amount. Instead, the whole system is altered, including the splitting of the quasi-Fermi levels and the electrical currents. The free energy gained by reducing one kind of loss is in a certain way apportioned between all other loss channels and the output power.

C. Application of the free energy loss analysis to a MWT-PERC

The free energy losses, according to Eqs. (21) and (22) and Eqs. (12)–(16), are given in Figure 4. Again, the analysis is based on the optical and numerical modeling of the MWT-PERC. As can be seen, many loss mechanisms are important. The recombination of charge carriers in the volume of the silicon crystal and at surfaces other than the effective contacts is negligible. Major loss mechanisms in terms of lost free energy flux are the transport of electrons, the reflection of light at the active cell area, recombination at the effective p- and n-type contacts, the transport of holes, and the

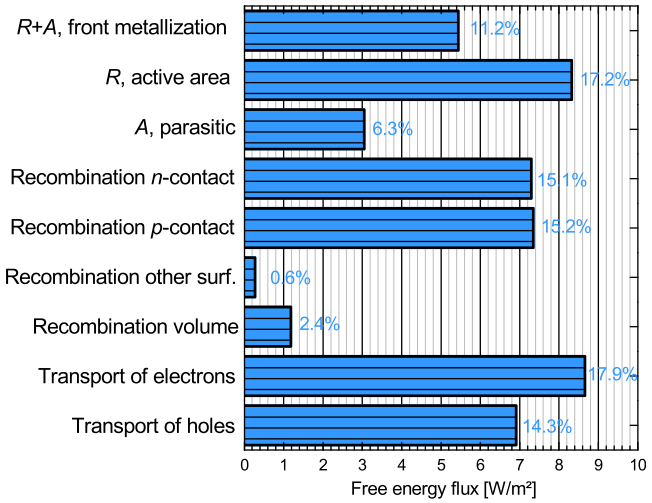

FIG. 4. The free energy loss analysis at the maximum power point shows that several loss channels are important for the analyzed MWT-PERC.

reflection and absorption at the front metallization. As expected, the optical losses are not over-represented, as is the case for the power balance (compare Figure 3). Since the losses are rather equally distributed, many aspects of the cell need to be improved in order to optimize the cell's energy conversion efficiency.

IV. SUMMARY

A method for a complete power balance is presented, which permits balancing the power incident on the solar cell, e.g., 1000 W/m^2 for standard test conditions, with the output power and the power losses. According to the proposed method, the lost power can be analyzed in terms of different optical, thermodynamic, and electrical mechanisms. The method relates the electrical output power, the fundamental losses, and technologically accessible losses to one another, giving interesting insights into the process of photovoltaic energy conversion. The power balance is exemplarily applied to a metal wrap through solar cell with passivated emitter and rear surface (MWT-PERC) showing that major losses occur due to thermalization of charge carriers and the generation of entropy.

Furthermore, a method for the analysis of the free energy losses, including optical and electrical effects, is presented. This method overcomes a weakness of the power balance method, i.e., the apparent over-representation of losses in the ultraviolet part of the solar spectrum, and thus eliminates potentially misleading hints for device optimization. The approach covers optical and electrical losses in terms of free energy, which is the usable amount of energy. Its application to the MWT-PERC shows that there is not a single loss mechanism dominating. Instead, several loss mechanisms are rather equally important.

ACKNOWLEDGMENTS

We acknowledge fruitful discussions with our colleagues M. Hermle and S. Glunz, and thank B. Thaidigsmann and E. Lohmüller for cell processing and characterization. J. Greulich and H. Höffler gratefully acknowledge the scholarship support of the German Federal Environmental Foundation (Deutsche Bundesstiftung Umwelt). This work is partially supported by the German Federal Ministry of Education and Research under Contract No. 03SF0335D ("xμ-Zellen Phase 2").

[1]W. Shockley and H. J. Queisser, J. Appl. Phys. **32**, 510 (1961).
[2]C. H. Henry, J. Appl. Phys. **51**, 4494 (1980).
[3]T. Tiedje, E. Yablonovitch, G. D. Cody, and B. G. Brooks, IEEE Trans. Electron Devices **31**, 711 (1984).
[4]M. A. Green, IEEE Trans. Electron Devices **31**, 671 (1984).
[5]M. J. Kerr, A. Cuevas, and P. Campbell, Prog. Photovoltaics **11**, 97 (2003).
[6]A. Richter, M. Hermle, and S. Glunz, IEEE J. Photovoltaics **3**, 1184 (2013).
[7]N. Huang, C. Lin, and M. L. Povinelli, J. Appl. Phys. **112**, 064321 (2012).
[8]R. Brendel, S. Dreissigacker, N. P. Harder, and P. P. Altermatt, Appl. Phys. Lett. **93**, 173503 (2008).
[9]R. Brendel, Prog. Photovoltaics **20**, 31 (2012).
[10]N. Brinkmann, G. Micard, Y. Schiele, G. Hahn, and B. Terheiden, Phys. Status Solidi (RRL) **7**, 322 (2013).
[11]F. Haase, S. Eidelloth, R. Horbelt, K. Bothe, E. G. Rojas, and R. Brendel, J. Appl. Phys. **110**, 124510 (2011).
[12]R. Brendel, J. H. Petermann, D. Zielke, H. Schulte-Huxel, M. Kessler, S. Gatz, S. Eidelloth, R. Bock, E. G. Rojas, J. Schmidt, and T. Dullweber, IEEE J. Photovoltaics **1**, 9 (2011).
[13]C. Mader, J. Müller, S. Eidelloth, and R. Brendel, Sol. Energy Mater. Sol. Cells **107**, 272 (2012).
[14]B. Thaidigsmann, J. Greulich, E. Lohmüller, S. Schmeißer, F. Clement, A. Wolf, D. Biro, and R. Preu, Sol. Energy Mater. Sol. Cells **106**, 89 (2012).
[15]E. Lohmüller, B. Thaidigsmann, M. Pospischil, U. Jäger, S. Mack, J. Specht, J. Nekarda, M. Retzlaff, A. Krieg, F. Clement, A. Wolf, D. Biro, and R. Preu, IEEE Electron Device Lett. **32**, 1719 (2011).
[16]IEC, "Photovoltaic devices - Part 3: Measurement principles for terrestrial photovoltaic (PV) solar devices with reference spectral irradiance data," 2nd ed. (International Electrotechnical Commission, Geneva, Switzerland, 2008), Vol. IEC 60904–3.
[17]J. Nelson, *The Physics of Solar Cells* (Imperial College Press, London, UK, 2003).
[18]P. Würfel, *Physics of Solar Cells - From Principles to New Concepts* (Wiley-Vch Verlag GmbH & Co. KgaA, Weinheim, Germany, 2005).
[19]R. K. Pathria and P. D. Beale, *Statistical Mechanics*, 3rd ed. (Elsevier, Oxford, UK, 2011).
[20]M. A. Green, J. Appl. Phys. **67**, 2944 (1990).
[21]E. Schneiderlöchner, R. Preu, R. Lüdemann, S. W. Glunz, and G. Willeke, *Laser-Fired Contacts (LFC)*, Munich, Germany, 2001 (WIP - Renewable Energies and ETA Florence), p. 1303.
[22]Sentaurus TCAD (Synopsys Inc., Mountain View, California, USA, 2010).
[23]J. Greulich, N. Wöhrle, M. Glatthaar, and S. Rein, Energy Procedia **27**, 234 (2012).
[24]N. Wöhrle, J. Greulich, C. Schwab, M. Glatthaar, and S. Rein, IEEE J. Photovoltaics **3**, 175 (2013).
[25]M. A. Green, Sol. Energy Mater. Sol. Cells **92**, 1305 (2008).
[26]M. Rüdiger, J. Greulich, A. Richter, and M. Hermle, IEEE Trans. Electron Devices **60**, 2156 (2013).
[27]A. Wolf, D. Biro, J.-F. Nekarda, S. Stumpp, A. Kimmerle, S. Mack, and R. Preu, J. Appl. Phys. **108**, 124510 (2010).